

Acute myeloid leukemia induces pro-tumoral p16INK4a driven senescence in the bone marrow microenvironment

Amina M Abdul-Aziz^{1*}, Yu Sun^{1*}, Charlotte Hellmich^{1*}, Christopher R Marlein¹, Jayna Mistry¹, Eoghan Forde¹, Rachel E Piddock¹, Manar S Shafat¹, Adam Morfakis¹, Tarang Mehta², Federica Di Palma^{1,2}, Iain Macaulay², Christopher J Ingham³, Anna Haestier⁴, Angela Collins⁷, Judith Campisi^{5,6}, **Kristian M. Bowles^{1,7}, **Stuart A Rushworth¹

¹Norwich Medical School, University of East Anglia, Norwich Research Park, Norwich, NR4 7UQ, United Kingdom.

²Earlham Institute, Norwich Research Park, Norwich, NR4 7UH, United Kingdom

³Department of Orthopaedic and Trauma Surgery, Norfolk and Norwich University Hospitals NHS Trust, Colney Lane, Norwich, NR4 7UY, United Kingdom

⁴Department of Obstetrics & Gynaecology, Norfolk and Norwich University Hospitals NHS Trust, Colney Lane, Norwich, NR4 7UY, United Kingdom

⁵Buck Institute for Research on Aging, 8001 Redwood Boulevard, Novato, CA 94945, USA

⁶Lawrence Berkeley National Laboratory, 1 Cyclotron Road, Berkeley, CA, 94720, USA

⁷Department of Haematology, Norfolk and Norwich University Hospitals NHS Trust, Colney Lane, Norwich, NR4 7UY, United Kingdom

* Denotes joint first author

**Denotes joint corresponding author

Running Title: AML drives bone marrow mediated p16INK4a senescence.

Corresponding authors: Dr Stuart Rushworth and Prof Kristian Bowles, Department of Molecular Haematology, Norwich Medical School, Norwich Research Park, Norwich, NR4 7UQ, United Kingdom. email: s.rushworth@uea.ac.uk and k.bowles@uea.ac.uk

Word count for text: 4127; abstract:103, Figure 5

Key points

- Leukemia blasts derived superoxide induces a senescent phenotype in cells within the bone marrow microenvironment
- Targeting the senescent bone marrow cells improves the survival of mice with leukemia.

Abstract

Acute myeloid leukemia (AML) is an age-related disease that is highly dependent on the bone marrow microenvironment. With increasing age, tissues accumulate senescent cells, characterized by an irreversible arrest of cell proliferation and the secretion of a set of pro-inflammatory cytokines, chemokines and growth factors, collectively known as the senescence-associated secretory phenotype (SASP). Here, we report that AML blasts induce a senescent phenotype in the stromal cells within the bone marrow microenvironment. We report that the bone marrow stromal cell senescence is driven by p16INK4a expression. The p16INK4a-expressing senescent stromal cells then feedback to promote AML blast survival and proliferation via the SASP. Importantly, selective elimination of p16INK4a-positive senescent bone marrow stromal cells *in vivo* improved the survival of mice with leukemia. Next, we find that the leukemia-driven senescent tumor microenvironment is caused by AML induced NOX2-derived superoxide. Finally, using the p16-3MR mouse model we show that by targeting NOX2 we reduced bone marrow stromal cell senescence and consequently reduced AML proliferation. Together, these data identify leukemia generated NOX2 derived superoxide as a driver of pro-tumoral p16INK4a-dependent senescence in bone marrow stromal cells. Our findings reveal the importance of a senescent microenvironment for the pathophysiology of leukemia. These data now open the door to investigate drugs which specifically target the 'benign' senescent cells that surround and support AML.

Acute myeloid leukemia (AML) is an age-related, often lethal disease that is highly dependent on the bone marrow (BM) microenvironment¹. Despite remission often seen after chemotherapy, long-term survival is modest. Thus, improved outcomes may depend on novel treatment strategies derived from a better understanding of the role of the BM in AML progression and relapse.

The BM is a structurally complex organ comprised of blood vessels and a heterogeneous population of cells that either directly participate in the generation of blood cells, or support the hematopoietic function of the tissue². Support cells in the BM all contribute to stimuli required for regulating normal hematopoiesis. In leukemia, however, the BM fails to produce adequate numbers of mature blood cells and platelets². Notably, AML blasts have been shown to alter the function of BM stromal cells (BMSC: including endothelial cells, fibroblasts and adipocytes)^{1,3-5}. This blast cell non-autonomous activity ultimately reshapes the BM microenvironment, thereby promoting AML tumor cell survival and proliferation.

Cellular senescence was described over 5 decades ago by Hayflick and colleagues⁶ as an irreversible arrest of normal cell proliferation. It is now clear that the senescence growth arrest evolved, at least in part, to suppress the development of cancer⁷. In addition to arrested growth, senescent cells show widespread changes in chromatin organization and gene expression⁸. These changes include the secretion of numerous pro-inflammatory cytokines, chemokines, growth factors and proteases, a feature termed the senescence-associated secretory phenotype (SASP)⁹. The senescence response, therefore, likely evolved not only to suppress the development of cancer, but also to aid tissue repair and regeneration in response to injury. However, because senescent cells gradually increase with age, the senescence response likely becomes maladaptive with age, and there is mounting evidence that they contribute to a variety of age-related phenotypes and pathologies^{7,10}. Furthermore, the SASP can disrupt a number of cellular and tissue functions, including, ironically, distinct pathologic pro-tumoral changes^{7,11}.

AML is primarily a disease of the elderly, with peak incidence between the ages of 80 and 85 years¹². Because AML is an age-related disease and highly dependent on the BM microenvironment, which naturally becomes senescent with age, we hypothesized, and subsequently tested the idea, that AML not only favors a senescent microenvironment but might actively shape a senescent micro-environment to promote tumor proliferation and survival.

Materials and Methods

Materials

Anti-p16 antibody was from BD Biosciences (Oxford, UK). Anti-humanCD45-BV421, anti-mouse CD45-human-BV421, anti-mouse CD31-PerCP, anti-mouse Ter119-APC, CD33-APC, anti-mouse CD45-PerCP anti-mouse CD140a APC-Cy7 and anti-mouse CD105-FITC were from Miltenyi Biotec (Bergisch Gladbach, Germany) and Biolegend (London, UK). All other reagents were obtained from Sigma-Aldrich (St Louis, MO, USA), unless otherwise indicated.

Methods

Cell cultures

Primary AML blasts and BMSCs were obtained from patient BMs (supplementary table 1). Non-senescent BMSCs were collected from the BM beneath the exposed acetabular surface of the pelvis during surgery of patients undergoing elective hip replacement. CD34+ cells were enriched from whole cord blood using CD34+ Magnetic Bead separation (Miltenyi Biotec). All tissue was taken following informed consent and under approval from the UK National Health Service Health Research Authority (LRECref07/H0310/146). For primary cell isolation, heparinized blood was isolated by density centrifugation using Histopaque as previously described¹³. Primary cells and cell lines were cultured in growth medium comprising DMEM, 10% FBS and 1% L-glutamine at 5% CO₂ at 37° C. BMSCs were isolated from hip replacement patients and AML bone marrow samples by adherence to tissue culture plastic and then expanded in DMEM containing 20% FBS plus 1% penicillin-streptomycin. BMSC markers were confirmed by flow cytometry for expression of CD90+, CD73+, CD105+ and CD45-.

Co-culture experiments

BMSC were seeded at 1×10^4 cells per well of a 4 well plate in normal growth media. BMSC were then transduced with either lentivirus containing control shRNA (shE) or test shRNA (p16 or p21) for 5 days. AML blasts (0.25×10^6) or normal CD34+ cells (0.25×10^6) were then co-cultured with the BMSC. Cells counts were based on hemocytometer counting and we used flow cytometry as a second test to confirm the cells were either AML (CD45+/CD33+) or CD34 (CD34+) of origin.

Senescence β -galactosidase assay

Senescence β -galactosidase staining kit (Cell Signaling Technology (CST), Massachusetts, USA) was used to detect SA-Bgal in BSMCs. BSMCs were cultured and treated in 35 mm dishes. The BSMCs were evaluated for the blue colour, indicative of SA- β gal positive cells.

Flow cytometry analysis and cell sorting

Cells were collected by centrifugation for 3 min at 400g washed and resuspended in phosphate-buffered saline (PBS), incubated for 5 min with the Fc receptor (FcR) blocking reagent, then stained with anti-human CD45-FITC, anti-mouse CD45-PerCP and anti-mouse CD105-APC antibodies or isotype controls. Analysis were performed on a CytoFLEX and using CytExpert analysis software (Bechman Coulter). Cell sorting was performed on a BD FACSMelody (BD Bioscience) and a BD Aria II cell sorter (BD Bioscience).

RNA extraction and real-time PCR

Total RNA was extracted from cells using the ReliaPrep RNA extraction kit from Promega (Southampton, UK) according to the manufacturer's instructions. Reverse transcription was performed using the qPCRBIO cDNA synthesis kit (PCR Biosystems, London, UK). Relative quantitative real-time PCR using qPCRBIO SyGreen Mix (PCR Biosystems, London, UK) was performed on cDNA generated from purified RNA. After pre-amplification (95°C for 2 min), the PCRs were amplified for 45 cycles (95°C for 15 sec, 60°C for 10 sec and 72°C for 10 sec) on a 384-well LightCycler 480 (Roche, Burgess Hill, UK). Each mRNA level was normalized against the beta-actin mRNA level.

Western immunoblotting and ELISAs

Western analyses following SDS-PAGE were carried out as described¹⁴. Briefly, whole cell lysates were extracted and SDS-PAGE gel electrophoresis separation performed. Western analysis performed using anti-p16INKa antibody; membranes were re-probed for beta-actin as a loading control.

shRNA silencing of p16, p21 and NOX2

Mission shRNA targeted lentivirus plasmids were purchased from Sigma-Aldrich. Control and targeted lentivirus stocks were produced as described¹⁵, concentrated using Amicon® Ultra centrifugal filters and titers determined using the Lenti-X™ qRT-PCR titration kit (CloneTech, Saint-Germain-en-Laye, France). BSMCs were infected with p16INK4a or p21 targeted virus. Knockdown was confirmed 5 days later and BSMCs were then combined with AML cells at a ratio of 1:5. MN1 cells were infected with NOX2 targeted virus. shRNA transduced cells were not sorted or enriched before use in experiments.

Retroviral AML transplantation mouse model

All animal experiments were performed in accordance with UK Home Office approvals and regulations and with approval from the Animal Welfare and Ethical Review Board of the University of East Anglia. C57BL/6J mice were obtained from Charles River (UK). In this study we also used p16-3MR mice developed by the Campisi lab¹⁶, which carry a transgene comprised of the p16INK4a regulatory elements driving expression of a fusion protein containing Renilla luciferase (to visualize p16INK4a expressing cells), monomeric red fluorescent protein (RFP; to visualize and isolate p16INK4a expressing cells) and the herpes simplex virus thymidine kinase (to selectively kill such cells by administering the pro-drug ganciclovir)¹⁶

Bone marrow was harvested from mice, and lineage-negative cells were obtained by negative selection using the Lineage Cell Depletion Kit (Miltenyi Biotec). Lineage-negative cells from C57BL/6J were retrovirally infected as previously described¹. To generate MN1 and HoxA9/Meis1 cells bone marrow cells were harvested from mice, and lineage-negative cells were obtained by negative selection using the Lineage Cell Depletion Kit (mouse) as recommended by the manufacturer (Miltenyi Biotec). Lineage-negative cells derived from C57BL/6J were retrovirally infected by co-culture with GP+E86 cells (ATCC) transfected with pSF91MN1iGFP, or MIG-HA-HoxA9 or MIY-HA-Meis1a (kindly provided by Professor Keith Humphries, Terry Fox Laboratory, Vancouver, Canada) in the presence of polybrene (10 µg/ml, Sigma-Aldrich)¹⁷. Co-culture with GP+E86 packaging pSF91MN1iGFP, MIG-HA-HoxA9 was performed for 3 days. MIH-HA-HoxA9 (GFP) transfected cells were then cocultured GP+E86 packaging MIY-HA-Meis1a (YFP) to generate HoxA9/Meis1 and MN1 overexpressing lineage negative cells. Cells were sorted using a FACS BD Aria II cell sorter. Cells were maintained in DMEM, 20% FCS supplemented with murine IL-3 (10ng/ml), murine IL-6 (10ng/ml) and murine SCF (100ng/ml) all purchased from PeproTech (London, UK). MN1 cells were then infected with pCDH-luciferase-T2A-mCherry, kindly provided by Prof. Irmela Jeremias, (Helmholtz Zentrum München, Munich, Germany)¹⁸. MN1 cells were plated at 5×10^4 /well in 12-well plates and expanded. MN1 cells expressing mCherry (MN1-luc) were sorted on a FACS Aria II cell sorter.

For AML induced senescence, 8-12 week old p16-3MR were injected with 1×10^5 MN1-luc expressing cells. To determine engraftment of MN1-luc cells into p16-3MR and C57BL/6 animals, mice were i.p. injected with luciferin (Fisher Scientific) and imaged for firefly luminescence (MN1-luc) using the In-vivo Bruker Xtreme (Coventry, UK). For survival experiments, MN1 engrafted p16-3MR mice were split into two groups before treatment with

GCV. Mice were then i.p. injected with GCV (25mg/kg) or PBS (control) for 5 consecutive days.

Primary AML and CD34⁺ hematopoietic progenitor cell xenograft model

NOD.Cg-Prkdcscid IL2rgtm1Wjl/SzJ (NSG) mice were obtained from The Jackson Laboratory (Bar Harbor, ME, USA). NSG mice were maintained under specific pathogen-free conditions. For the AML xenograft model, 2×10^6 viable primary AML cells were washed and resuspended in PBS. Cells were then injected into the tail vein of non-irradiated 6-8 week old female NSG mice. When clinical signs of illness were apparent (rough fur, hunchback, or reduced motility) or if 12 weeks post injection was reached, mice were sacrificed by exposure to CO₂. For the CD34⁺ hematopoietic progenitor cell (HPC) xenograft model (hu-NSG) 2×10^5 CD34⁺ cord blood cells were injected into the tail vein of non-irradiated 3-4 week old female NSG. CD34⁺ cell engraftment was monitored peripheral blood analysis for human CD45 cells. 12 weeks post injection mice were sacrificed by exposure to CO₂. BM was harvested and cell sorting was performed for human CD45- and mouse CD45-, Ter119-, CD31-, CD105+, CD140a+. BM was also analysed for human cell engraftment by human CD45+ cells. If more than 1% of human CD45 cells were detected in the BM, the AML sample was determined to be engrafted.

Statistical analyses

The Mann-Whitney U test was used to compare test groups where stated. $p < 0.05$ was considered statistically significant and denoted by *. Results were the mean \pm standard deviation of four or more independent experiments. We generated statistics using Graphpad Prism5 software (Graphpad, San Diego, CA, USA). For Western analyses, data are representative images of three independent experiments.

Results

AML induces a senescent phenotype *in vivo*.

We showed that primary human AML cells induce a SASP (upregulation of IL-6, IL-8, MIP1a and MIP3a) when co-cultured with primary BMSCs⁴. Here, we determined whether AML cells can induce a SASP *in vivo*. We engrafted 4 primary AML patient-derived cells (AML-NSG) and normal human cord blood derived CD34+ HPC (hu-NSG) into immunocompromised NSG mice by tail vein injection (schematic, Figure 1A). Ten-12 weeks after injection, we sacrificed the animals; we determined engraftment (Figure 1B), sorting CD45 negative (mouse and human), CD31 negative, Ter119 negative, CD140a positive and CD105 positive BMSCs (Figure 1C). The frequency of BMSCs in hu-NSG compared to AML-NSG is shown in supplementary figure 1. Mouse BMSCs (mBMSCs) from hu-NSG served as a negative control. Sorted BMSC from hu-NSG and AML-NSG were analyzed for gene expression by real-time PCR. Our analyses showed that the expression of p16INK4a, and to a lesser extent p21, was consistently up-regulated in mBMSCs from AML cell engrafted mice (Figure 1D). Further, the SASP components IL-6 and MIP3, although not MIP1a, were also consistently up-regulated in mBMSCs from animals engrafted with leukemic cells compared to animals engrafted with human CD34+ HPC (Figure 1E). Loss of lamin B1 is another identifier of senescent cells¹⁹. Consistent with the expression of p16INK4a, IL-6 and MIP1a, lamin B expression declined in BMSCs from AML engrafted NSG mice (Figure 1F). Plasma concentrations of mouse IL-6 are also elevated in AML-NSG mice compared to hu-NSG mice (Figure 1G). Mouse MIP3 concentrations were undetected in both treatment groups. Together, these data suggest that AML cells can induce a senescent phenotype in the BM microenvironment.

BMSC senescence is driven by p16INK4a-expressing cells and is pro-tumoral

To determine the drivers of AML-induced senescence in human BMSCs, we cultured primary AML cells or normal CD34+ HPC with human primary non-senescent BMSCs for 6 days. Human BMSCs were then assayed for senescence-associated β -Galactosidase (SA-Bgal), IL-6 and lamin B1. Human BMSCs co-cultured with AML cells showed increased SA-Bgal staining (Figure 2A, B), increased IL-6 and IL-8 expression (Figure 2C) and reduced lamin B1 expression (not shown) compared to BMSCs co-cultured with normal CD34+ HPC, consistent with AML-induced cellular senescence. Co-culture with AML cells also induced p16INK4a and p21 expression in BMSCs (Figure 2D). Subsequently, we examined the impact of p16INK4a or p21 knockdown (Supplementary Figure 2A, B and C) in human BMSCs on AML cell or normal CD34+ HPC survival. AML cells showed reduced growth, as determined by cell number, when co-cultured on p16 knockdown BMSCs (Figure 2E and supplementary figure 2C). In addition, knockdown of p16INK4a in BMSC prevented

senescence when cultured with AML (Figure 2F). We conclude that p16 driven senescence in human BMSCs is pro-tumoral.

Deleting BM senescent cells reduces tumor growth

A number of murine models have been developed to study p16INK4a driven senescence *in vivo*^{16,20,21}. We used p16-3MR mice, which carry a transgene comprised of the p16INK4a regulatory elements driving expression of a fusion protein containing Renilla luciferase (to visualize p16INK4a expressing cells), monomeric red fluorescent protein (RFP; to isolate such cells) and the herpes simplex virus thymidine kinase (to selectively kill such cells by administering the pro-drug ganciclovir) (Figure 3A)¹⁶.

To determine whether AML induces senescence in p16-3MR mice, we isolated BMSCs from these mice and co-cultured them with MN1 cells, (mouse myeloid leukemic cells), HoxA9/Meis1 (mouse myeloid leukemic cells) or lineage negative cells (lin-) for 6 days, as this incubation time has been shown to increase RFP in cells from the p16-3MR model under injury¹⁶. After 6 days of co-culture, p16-3MR BMSCs cultured with MN1 or HoxA9/Meis1 cells but not lineage negative cells had detectable red fluorescence (Figure 3B-C), consistent with p16INK4a-driven senescence. To confirm senescence in the p16-3MR BMSCs, we examined p16INK4a protein levels and showed that under co-culture conditions p16-3MR BMSCs had elevated levels of p16INK4a protein, and this increase did not depend on direct cell-cell contact (Figure 3D). Moreover, conditioned media from MN1 also increased p16INK4a protein expression in BMSC, whereas co-culture of BMSCs with lineage negative cells had no effect on p16INK4a protein expression (Figure 3E). This finding suggests that the AML signal which drives BMSCs into senescence is soluble.

To determine whether AML engraftment induces senescence in the p16-3MR BM *in vivo*, first we transfected MN1 cells with firefly luciferase (MN1-luc) to detect their presence after engraftment into p16-3MR mice (Supplementary figure 3). Next, firefly luciferase activity confirmed engraftment of MN1 into p16-3MR mice. Finally, we examined BMSCs from the BM of p16-3MR animals engrafted with MN1 for RFP (Figure 3F, G). MN1 cells induced RFP expression in p16-3MR mice compared to control animals, consistent with the AML cells inducing a senescence response.

Next, we created senescent p16-3MR BMSCs by culturing them with MN1 cells in transwells for 6 days. We then treated the co-cultures with ganciclovir (GCV) (Figure 4A). MN1 cells showed reduced cell number when cultured on senescent BMSCs treated with GCV compared to BMSCs treated with PBS. To test the hypothesis that senescent BMSCs fuel tumorigenesis *in vivo*, we injected MN1 cells into p16-3MR mice, followed by GCV treatment (Figure 4B). p16-3MR mice engrafted with MN1-luc cells for 14 days, then treated with GCV (once daily for 5 days), showed reduced tumor load compared to PBS treated p16-

3MR mice engrafted with MN1-luc cells (Figures 4C,D). Tumor load was detected by firefly luciferase expressed from MN1-luc cells which is activated by the substrate luciferin, and not coelenterazine which activates luciferase derived from Renilla (supplementary figure 3). Moreover, MN1-luc engrafted p16-3MR mice survived longer following five days of GCV treatment compared to control treated animals (Figure 4E). Finally, to confirm that this survival was due to the GCV effect of the p16-3MR transgene and not a direct effect of GCV, we engrafted MN1-luc cells into non-transgenic C57BL/6 animals (Figure 4F). GCV had no effect on C57BL/6 mice engrafted with MN1-luc cells. Furthermore, GCV reduced RFP expressing BSMC cells *in-vivo* in p16-3MR mice engrafted with MN1 cells and reduced b-gal staining in BMSC cultured with MN1 cells *in vitro* (supplementary figure 4A and B). We conclude that deletion of senescent non-malignant BMSCs is anti-leukemic.

NOX2 derived superoxide drives AML associated BM senescence

By what mechanism do AML cells induce senescence in BMSCs? One established inducer of senescence is oxidative stress^{22,23}, and we showed that human AML cells induce oxidative stress in BMSCs²⁴. Indeed, MN1 and HoxA9/Meis1 cells, but not lineage negative cells, increased oxidative stress as measured by increased DCF (dihydrodichlorofluorescein diacetate, detect cellular ROS level) fluorescence in BMSCs from p16-3MR mice (Figure 5A). Supplementary figure 5 shows that human primary AML, but not normal CD34+ HPC, can induce ROS in BMSC. AML blasts were reported to generate more superoxide than nonmalignant CD34+ cells²⁵. This ROS was a consequence of superoxide generated by NOX2, which was shown to benefit malignant cells^{24,25}. Moreover, ROS in the form of H₂O₂ can induce senescence in several cell types^{22,23}. Therefore, we determined whether H₂O₂ induced senescence in BMSCs in culture. Indeed, treating human BMSCs with H₂O₂ induced a senescent phenotype (Figure 5B, C). Importantly, after MN1 cells were injected into allogeneic mice, hydrogen peroxide levels as measured by the Amplex Red Assay were elevated in the whole BM, a phenomenon that did not occur in control mice (Figure 5D). Moreover, ROS levels, analysed by flow cytometry, in BMSCs also increased in MN1 engrafted mice (Figure 5E).

Finally, we asked whether AML derived NOX2 dependent superoxide is responsible for inducing p16INK4a-driven senescence in p16-3MR mice. We depleted NOX2 from MN1 cells (Figure 5F). Strikingly, we found increased survival of p16-3MR mice engrafted with MN1 cells with NOX2 knockdown compared to control knockdown animals (Figure 5G). Moreover, BMSC cultured with NOX-KD cells had reduced levels of ROS compared to control-KD MN1 cells (supplementary 6A). Knockdown of NOX2 in MN1 cells engrafted into p16-3MR mice also resulted in significantly fewer senescent BMSCs (Figure 5H and supplementary figure 6B). Moreover, when we treat NOX2-KD MN1 engrafted p16-3MR

mice with GCV no additive affect is observed (Figure 5I). Together, these data identify AML generated NOX2 derived superoxide as a driver of p16INK4a-dependent senescence.

Discussion

Here we report that AML cells induce a SASP in the BM microenvironment, which supports the survival and proliferation of the leukemic blasts. *In vivo*, AML cells induce senescence in BMSC. Deletion of these senescent p16INK4a-expressing BMSCs slows tumor progression and extends animal survival. Notably, the senescence response and SASP is driven by superoxide generated locally by the tumor.

AML is primarily a disease of the elderly. The Swedish Adult Acute Leukemia Registry reported that the highest incidence of AML occurred between the ages 80 to 85 years, with a median age at diagnosis of 72 years¹². Outcomes for older patients with AML are poor. However, this poor prognosis is not sufficiently explained by more frequent adverse prognostic factors or genetic complexities of the tumor¹². In a comparison between younger and older patients enrolled in the UK MRC AML 10 (age < 55 years at diagnosis)²⁶ and AML 11 (aged 60+ years)²⁷ clinical trials, Grimwade and colleagues found that the poorer survival of older patients with favorable cytogenetic abnormalities, compared with younger individuals with similar genetic lesions, could not be accounted for by the frequency, nature or number of secondary aberrations. Rather, the deleterious effect of advancing age at time of diagnosis remained a highly significant prognostic factor even after hierarchical cytogenetic risk group was taken into account²⁸. The causes for the poorer prognosis of older patients compared with younger patients with similar leukemia cell biologic features are likely many but are not yet completely explained. These observations however are consistent with the hypothesis that biological differences in the older versus younger tumor host environment contribute to poorer outcomes in older patients. Our findings show that AML induces senescence in the BM microenvironment of the host and that this in turn was pro-tumoral. We therefore hypothesize that a senescent microenvironment (which also occurs with aging) may contribute to these clinical observations.

We observed that both p16INK4a and p21 are up-regulated in BMSCs from mice engrafted with human AML cells. Other studies showed that mice with single p16INK4a or p21 knockout are still capable of senescence because of compensatory actions of p16INK4a and p21. However, cells from double knockout mice show little or no senescence^{16,29}. Using the p16-3MR mouse model to generate an *in vivo* model of the mouse AML microenvironment, we show that induction of p16INK4a expression in BMSCs was sufficient to generate senescence and promote progression AML tumor progression. Knockdown of p21 had no significant effect on AML tumor volume in our studies.

Other *in vivo* models of p16INK4a senescence^{20,21} showed that expression of p16INK4a with age does not necessarily predict overall cancer development, suggesting that the accumulation of senescent cells is not a principal determinant of cancer-related death. In these studies, p16INK4a activation was observed in emerging neoplasms, as well as surrounding stromal cells in 5/5 solid tumor models studied. Such data suggests that, while maybe not sufficient to cause malignancy, p16INK4a activation is a characteristic of emerging cancer. Conversely, others have shown that the elimination of senescent cells during aging in mice produces smaller and presumably less aggressive tumors³⁰, and that cancer associated fibroblasts from breast tumors have a proliferative phenotype and associated low p16INK4a expression compared to non-cancer associated fibroblasts³¹. Thus, the presence of senescent stromal cells may be tumor specific. Here we add AML to the list of diseases in which p16INK4a activation in cancer associated stromal cells is pro-tumoral.

Using p16-3MR mice, we show that AML induces a senescent BM phenotype through superoxide derived from the tumor. ROS are known to induce senescence in both benign and malignant tissue^{9,11,22}. Moreover, most cancers have been shown to produce ROS³². We and others showed that NOX2-derived superoxide drives part of the malignant phenotype of AML^{24,25}. Because the known stimuli of cellular senescence include DNA damage and ROS^{33,34}, we investigated whether the SASP in the BM microenvironment, occurring in response to AML, was a consequence of AML induced superoxide. We found that ROS drives BM cellular senescence through BMSC p16INK4a expression. Furthermore, using p16-3MR mice, we showed that targeting NOX2 impaired BMSC senescence and leukemic proliferation.

Cellular senescence is emerging as a fundamental and complex component of both health and disease³⁵. Senescence is a response to cellular damage, which results in irreversible cell cycle arrest and subsequent secretion of cytokines, chemokines and other factors known as the SASP^{11,36}. The beneficial functions of senescence include the promotion of tissue repair, wound healing and tumor suppression^{16,37,38}. In addition, senescent cells naturally accumulate with age and contribute to the pathophysiology of a spectrum of age related disorders including cancers, atherosclerosis and osteoarthritis³⁶. In an apparent paradox, it is increasingly recognized that cellular senescence underpins a number of both degenerative and hyperplastic diseases of aging⁷. Therapeutically, clearance of senescent cells from the microenvironment has been reported to attenuate the effects of age related degenerative illness and result in a regenerative program of healing in a model of osteoarthritis³⁹. Such data promote the hypothesis that drug targeting of

senescent cells might improve current treatments (and outcomes) more broadly for patients with degenerative disorders. Similarly, the data presented here, and by others⁴⁰, linking senescent cells in the leukemia microenvironment to the malignant phenotype of AML, suggests that chemotherapeutic strategies, which include targeting of senescent cells in the microenvironment, may benefit patients with leukemia through either direct effects on tumor development and/or by enhancing responses to tumor directed chemotherapy drugs.

P16INK4a regulates the cell cycle by slowing progression from G1 to S phase. In one enforced expression model of p16INK4a, several components of the SASP were independent of p16INK4a expression, so several aspects of the SASP are considered a damage response that is separable from the growth arrest⁴¹. Nevertheless, both the SASP and growth arrest occurred as a consequence of ROS mediated p16INK4a activation⁴¹. Here we show that p16INK4a driven BMSC senescence is a consequence of increased ROS generated by malignant cells. Whether the SASP component of senescence is directly downstream of p16INK4a or mediated through alternate pathways in response to ROS is not clear. It is, however, the case that deletion of p16INK4a expressing senescent cells in the tumor microenvironment directly inhibits AML growth and improves animal survival.

In summary, our results describe the pro-tumoral pathophysiologic consequences of leukemia-induced cellular senescence in the BM microenvironment and the mechanism by which this occurs. Our data open the door to future studies investigating the utility of compounds, not targeting the malignant cell, but targeting the 'benign' senescent cells that surround and support the tumor.

Acknowledgements

The authors wish to thank the Norwich Research Park (NRP), Ministry of Higher Education and Scientific Research of the State of Libya, The Big C cancer charity (Norfolk, UK), The Rosetrees Trust and The National Institute for Health Research (UK) and the US National Institutes of Health (National Institute on Aging) and Larry L. Hillblom foundation for funding and Professor Richard Ball, Dr Mark Wilkinson and Mr Iain Sheriffs, Norwich Biorepository (UK) for help with sample collection and storage. pCDH-luciferase-T2A-mCherry was kindly gifted by Professor Irmela Jeremias, MD, from Helmholtz Zentrum München, Munich, Germany. The authors also thank Dr Allyson Tyler, Dr Ian Thirkettle and Dr Karen Ashurst from the Laboratory Medicine department at the Norfolk and Norwich University Hospital for technical assistance.

Author Contribution

A.A.A., C.H., Y.S., K.M.B and S.A.R designed the research; A.A.A., C.H., Y.S., C.R.M., R.E.P., I.M., E.F., J.M., A.M., and M.S.S., performed the research; S.A.R., C.H., Y.S., C.R.M. and R.E.P. carried out in vivo work; J.C., T.M., F.D., C.J.I., A.C., A.H., and K.M.B. provided essential reagents and knowledge. A.A.A., C.H., Y.S., K.M.B., and S.A.R. wrote the paper, with edits from J.C.

Conflict of interests

The authors declare no competing interests

References

1. Shafat MS, Oellerich T, Mohr S, et al. Leukemic blasts program bone marrow adipocytes to generate a protumoral microenvironment. *Blood*. 2017;129(10):1320-1332.
2. Miraki-Moud F, Anjos-Afonso F, Hodby KA, et al. Acute myeloid leukemia does not deplete normal hematopoietic stem cells but induces cytopenias by impeding their differentiation. *Proc Natl Acad Sci U S A*. 2013;110(33):13576-13581.
3. Pezeshkian B, Donnelly C, Tamburo K, Geddes T, Madlambayan GJ. Leukemia Mediated Endothelial Cell Activation Modulates Leukemia Cell Susceptibility to Chemotherapy through a Positive Feedback Loop Mechanism. *PLoS One*. 2013;8(4):e60823.
4. Abdul-Aziz AM, Shafat MS, Mehta TK, et al. MIF-Induced Stromal PKCbeta/IL8 Is Essential in Human Acute Myeloid Leukemia. *Cancer Res*. 2017;77(2):303-311.
5. Rynningen A, Wergeland L, Glenjen N, Gjertsen BT, Bruserud O. In vitro crosstalk between fibroblasts and native human acute myelogenous leukemia (AML) blasts via local cytokine networks results in increased proliferation and decreased apoptosis of AML cells as well as increased levels of proangiogenic Interleukin 8. *Leuk Res*. 2005;29(2):185-196.
6. Hayflick L. The biology of human aging. *Am J Med Sci*. 1973;265(6):432-445.
7. Campisi J. Aging, cellular senescence, and cancer. *Annu Rev Physiol*. 2013;75:685-705.
8. Salama R, Sadaie M, Hoare M, Narita M. Cellular senescence and its effector programs. *Genes Dev*. 2014;28(2):99-114.
9. Coppe JP, Patil CK, Rodier F, et al. Senescence-associated secretory phenotypes reveal cell-nonautonomous functions of oncogenic RAS and the p53 tumor suppressor. *PLoS Biol*. 2008;6(12):2853-2868.
10. de Keizer PL. The Fountain of Youth by Targeting Senescent Cells? *Trends Mol Med*. 2017;23(1):6-17.
11. Munoz-Espin D, Serrano M. Cellular senescence: from physiology to pathology. *Nat Rev Mol Cell Biol*. 2014;15(7):482-496.
12. Juliusson G, Antunovic P, Derolf A, et al. Age and acute myeloid leukemia: real world data on decision to treat and outcomes from the Swedish Acute Leukemia Registry. *Blood*. 2009;113(18):4179-4187.
13. Zaitseva L, Murray MY, Shafat MS, et al. Ibrutinib inhibits SDF1/CXCR4 mediated migration in AML. *Oncotarget*. 2014;5(20):9930-9938.
14. Pillinger G, Abdul-Aziz A, Zaitseva L, et al. Targeting BTK for the treatment of FLT3-ITD mutated acute myeloid leukemia. *Sci Rep*. 2015;5:12949.
15. Rushworth SA, Zaitseva L, Murray MY, Shah NM, Bowles KM, MacEwan DJ. The high Nrf2 expression in human acute myeloid leukemia is driven by NF- κ B and underlies its chemo-resistance. *Blood*. 2012;120:5188-5198.
16. Demaria M, Ohtani N, Youssef SA, et al. An essential role for senescent cells in optimal wound healing through secretion of PDGF-AA. *Dev Cell*. 2014;31(6):722-733.
17. Heuser M, Argiropoulos B, Kuchenbauer F, et al. MN1 overexpression induces acute myeloid leukemia in mice and predicts ATRA resistance in patients with AML. *Blood*. 2007;110(5):1639-1647.
18. Vick B, Rothenberg M, Sandhöfer N, et al. An Advanced Preclinical Mouse Model for Acute Myeloid Leukemia Using Patients' Cells of Various Genetic Subgroups and *In Vivo* Bioluminescence Imaging. *PLoS ONE*. 2015;10(3):e0120925.
19. Freund A, Laberge RM, Demaria M, Campisi J. Lamin B1 loss is a senescence-associated biomarker. *Mol Biol Cell*. 2012;23(11):2066-2075.
20. Burd CE, Sorrentino JA, Clark KS, et al. Monitoring tumorigenesis and senescence in vivo with a p16(INK4a)-luciferase model. *Cell*. 2013;152(1-2):340-351.
21. Baker DJ, Wijshake T, Tchkonia T, et al. Clearance of p16Ink4a-positive senescent cells delays ageing-associated disorders. *Nature*. 2011;479(7372):232-236.

22. Sasaki M, Kajiya H, Ozeki S, Okabe K, Ikebe T. Reactive oxygen species promotes cellular senescence in normal human epidermal keratinocytes through epigenetic regulation of p16(INK4a.). *Biochem Biophys Res Commun.* 2014;452(3):622-628.
23. Zhang Y, Zhang Y, Zhong C, Xiao F. Cr(VI) induces premature senescence through ROS-mediated p53 pathway in L-02 hepatocytes. *Scientific Reports.* 2016;6:34578.
24. Marlein CR, Zaitseva L, Piddock RE, et al. NADPH oxidase-2 derived superoxide drives mitochondrial transfer from bone marrow stromal cells to leukemic blasts. *Blood.* 2017;130(14):1649-1660.
25. Hole PS, Zabkiewicz J, Munje C, et al. Overproduction of NOX-derived ROS in AML promotes proliferation and is associated with defective oxidative stress signaling. *Blood.* 2013;122(19):3322-3330.
26. Grimwade D, Walker H, Oliver F, et al. The importance of diagnostic cytogenetics on outcome in AML: analysis of 1,612 patients entered into the MRC AML 10 trial. The Medical Research Council Adult and Children's Leukaemia Working Parties. *Blood.* 1998;92(7):2322-2333.
27. Wheatley K, Brookes CL, Howman AJ, et al. Prognostic factor analysis of the survival of elderly patients with AML in the MRC AML11 and LRF AML14 trials. *Br J Haematol.* 2009;145(5):598-605.
28. Grimwade D, Walker H, Harrison G, et al. The predictive value of hierarchical cytogenetic classification in older adults with acute myeloid leukemia (AML): analysis of 1065 patients entered into the United Kingdom Medical Research Council AML11 trial. *Blood.* 2001;98(5):1312-1320.
29. Takeuchi S, Takahashi A, Motoi N, et al. Intrinsic cooperation between p16INK4a and p21Waf1/Cip1 in the onset of cellular senescence and tumor suppression in vivo. *Cancer Res.* 2010;70(22):9381-9390.
30. Baker DJ, Childs BG, Durik M, et al. Naturally occurring p16(Ink4a)-positive cells shorten healthy lifespan. *Nature.* 2016;530(7589):184-189.
31. Al-Ansari MM, Hendrayani SF, Shehata AI, Aboussekhra A. p16(INK4A) Represses the paracrine tumor-promoting effects of breast stromal fibroblasts. *Oncogene.* 2013;32(18):2356-2364.
32. Michalak KP, Mackowska-Kedziora A, Sobolewski B, Wozniak P. Key Roles of Glutamine Pathways in Reprogramming the Cancer Metabolism. *Oxid Med Cell Longev.* 2015;2015:964321.
33. Chen QM, Bartholomew JC, Campisi J, Acosta M, Reagan JD, Ames BN. Molecular analysis of H2O2-induced senescent-like growth arrest in normal human fibroblasts: p53 and Rb control G1 arrest but not cell replication. *Biochemical Journal.* 1998;332(Pt 1):43-50.
34. Rodier F, Coppe JP, Patil CK, et al. Persistent DNA damage signalling triggers senescence-associated inflammatory cytokine secretion. *Nat Cell Biol.* 2009;11(8):973-979.
35. He S, Sharpless NE. Senescence in Health and Disease. *Cell.* 2017;169(6):1000-1011.
36. Freund A, Orjalo AV, Desprez PY, Campisi J. Inflammatory networks during cellular senescence: causes and consequences. *Trends Mol Med.* 2010;16(5):238-246.
37. Perez-Mancera PA, Young AR, Narita M. Inside and out: the activities of senescence in cancer. *Nat Rev Cancer.* 2014;14(8):547-558.
38. Ritschka B, Storer M, Mas A, et al. The senescence-associated secretory phenotype induces cellular plasticity and tissue regeneration. *Genes Dev.* 2017;31(2):172-183.
39. Jeon OH, Kim C, Laberge RM, et al. Local clearance of senescent cells attenuates the development of post-traumatic osteoarthritis and creates a pro-regenerative environment. *Nat Med.* 2017;23(6):775-781.
40. Geyh S, Rodriguez-Paredes M, Jager P, et al. Functional inhibition of mesenchymal stromal cells in acute myeloid leukemia. *Leukemia.* 2016;30(3):683-691.
41. Coppe JP, Rodier F, Patil CK, Freund A, Desprez PY, Campisi J. Tumor suppressor and aging biomarker p16(INK4a) induces cellular senescence without the associated inflammatory secretory phenotype. *J Biol Chem.* 2011;286(42):36396-36403.

Figure legends:

Figure 1. Primary human AML induces a p16 driven SASP *in vivo*. (A) Schematic of *in vivo* experiment in which 2×10^6 primary AML cells (4 individual patient AML and 5 CD34 HPC) were injected into NSG mice. (B) Engraftment was measured by detecting human CD45 by flow cytometry. In the dot plot each AML engraftment into NSG mice is shown for bone marrow. (C) Representative gating strategy for BMSC cell (hCD45-, mCD45-, mCD31-, mTer119-, mCD105+, mCD140a+) population which was sorted. (D) RNA analysis for p16 and p21 in the sorted BMSC (hCD45-, mCD45-, mCD31-, mTer119-, mCD105+, mCD140a+) isolated from NSG mice engrafted with primary human AML or cord blood CD34+ HPC (E) RNA analysis for SASP in the sorted BMSC. (F) RNA analysis for lamin B in the sorted BMSC. (G) Terminal peripheral blood samples were taken and plasma isolated from all NSG mice engrafted with primary human AML or cord blood CD34+ HPC and mouse IL-6 was measured by ELISA. The Mann-Whitney U test was used to compare between treatment groups (* = $p < 0.05$).

Figure 2. AML induced senescence in BMSC. (A) BMSC were cultured alone or with primary AML (0.25×10^6 n=12) or with CD34+ HPC (0.25×10^6 n=7) for 6 days. Non-adherent cells were removed and BMSC were analysed for senescence associated B-Galactosidase staining (SA- β -gal). (B) Bar graph representation of SA- β -gal positive cells from Figure 2A. (C) BMSC were cultured alone or with primary AML (0.25×10^6 n=10) or with CD34+ HPC (0.25×10^6 n=5) for 6 days. Non-adherent cells were removed and RNA was extracted from the BMSC. RNA was analysed for IL-6 and IL-8 expression using qRT-PCR. (D) As for (C) but analyzed for p16 and p21. (E) BMSC were infected with p16 targeted shRNA or control shRNA lentivirus and cultured for 5 days. AML blasts (0.25×10^6 n=10) or CD34+ HPC (0.25×10^6 n=5) were co-cultured with BMSC with control shRNA or on BMSC with p16 shRNA. AML blast number was assessed using a trypan blue exclusion hemocytometer-based counts and CD33/CD45+ staining using flow cytometry. (F) To confirm the senescent profile of BMSC from (E) non-adherent cells were removed and BMSC were analysed for senescence associated B-Galactosidase staining (SA- β -gal) (n=5). The Mann-Whitney U test was used to compare between treatment groups (* = $p < 0.05$). Each dot on the dot plots represents a different AML or CD34 HPC sample.

Figure 3. MN1 engraftment drives p16-3MR. (A) Schematic of p16-3MR model. (B) Fluorescent images of p16-3MR isolated BMSC which have been cultured alone or with lineage negative cells (lin-), MN1 cells or HoxA9/Meis1 cells for 6 days. (n=3) (C) Flow cytometry analysis of p16-3MR BMSC which have been cultured alone or with lineage

negative cells (lin-), MN1 cells or HoxA9/Meis1 cells for 6 days. (n=3) (D) Western blot analysis of p16-3MR BMSC cultured alone or with MN1 for 6 days (DC = direct contact or TW - transwell). Blots were reprobated with B-actin to confirm sample loading (shown are representative images of 3 blots). (E) Western blot analysis of p16-3MR BMSC cultured alone or with lineage negative cells (lin-), conditioned media (CM) from MN1 cells or MN1 cells. Blots were reprobated with B-actin to confirm sample loading (shown are representative images of 3 blots) (F) 1×10^5 MN1 cells were injected into the tail vein of p16-3MR mice. BM was isolated and analysed for mouse BMSC (mCD45-, mCD31-, mTer119-, mCD105+, mCD140a+) expressing red fluorescent protein (RFP) using flow cytometry (n=5). (G) Flow cytometry analysis of p16-3MR BMSC measuring RFP (F). The Mann-Whitney U test was used to compare between treatment groups (* = $p < 0.05$).

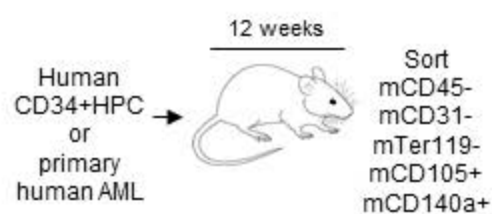
Figure 4. Deleting senescent cells reduces AML tumor volume. (A) MN1 were grown on p16-3MR non-senescent or senescent BMSC for 2 days with and without treatment with GCV (10 μ g/ml) (n=3). (B) schematic of GCV experiment *in vivo*. (C and D) 1×10^5 MN1-luc cells were injected into p16-3MR mice (n=8 for each treatment group). Mice were imaged at 14 days post engraftment. At day 15, GCV (25mg/kg) or PBS treatment was started for 5 days. Mice were then imaged again 1 day after GCV treatment had finished. Pre and post images show the same mice in the same order (C). (D). Densitometry of the bioluminescent images was performed to determine differences between vehicle and GCV treated animals. (E and F) Kaplan-Meier survival curves for p16-3MR (n=8) and C57BL/6 (n=7) mice injected with MN1 and then treated with vehicle or GCV as shown in (B).

Figure 5. AML-induced NOX2 derived superoxide drives BM senescence. (A) BMSC from p16-3MR were isolated and then cultured alone or with lineage negative cells, MN1 cells or HoxA9/Meis1 cells for 3 days. DCF fluorescence was assessed in BMSC by flow cytometry (n=4). (B) human BMSC were treated with 10 μ M H₂O₂ for 6 days and then analysed for senescence associated B-Galactosidase staining (SA- β -gal), and (C) p16 mRNA expression (n=4). (D) C57BL/6 mice injected with MN1. At 21 days post engraftment mice were sacrificed and whole BM was isolated and analysed for H₂O₂ production using the amplex red assay (n=5). (E) C57BL/6 mice were injected with MN1 cells. At 21 days post engraftment mice were sacrificed and BMSC were analysed by flow cytometry for DCF fluorescence (n=5). (F) Real-time PCR assay was used to analyse the NOX2 mRNA expression level in NOX2-KD MN1 cells compare to control-KD cells (n=4). (G) Kaplan-Meier survival curves for p16-3MR mice injected with MN1 NOX2-KD cells or MN1 control-KD cells (n=7 in each group). (H) At the end point of the experiment BM was isolated and

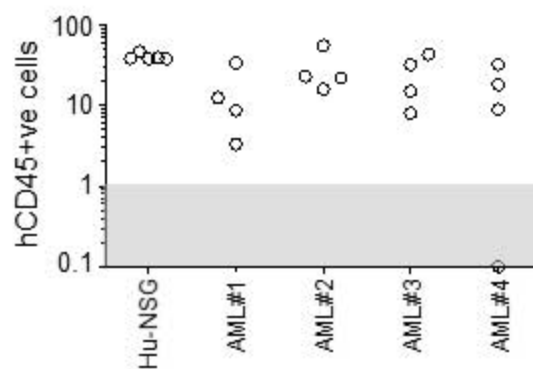
flow cytometry was performed to detect BMSC derived RFP (n=5). (I) Kaplan-Meier survival curves for p16-3MR mice injected with MN1 NOX2-KD cells or MN1 control-KD cells and then i.p. injected with PBS or GCV at day 15, GCV (25mg/kg) for 5 days (n=4).

Figure 1.

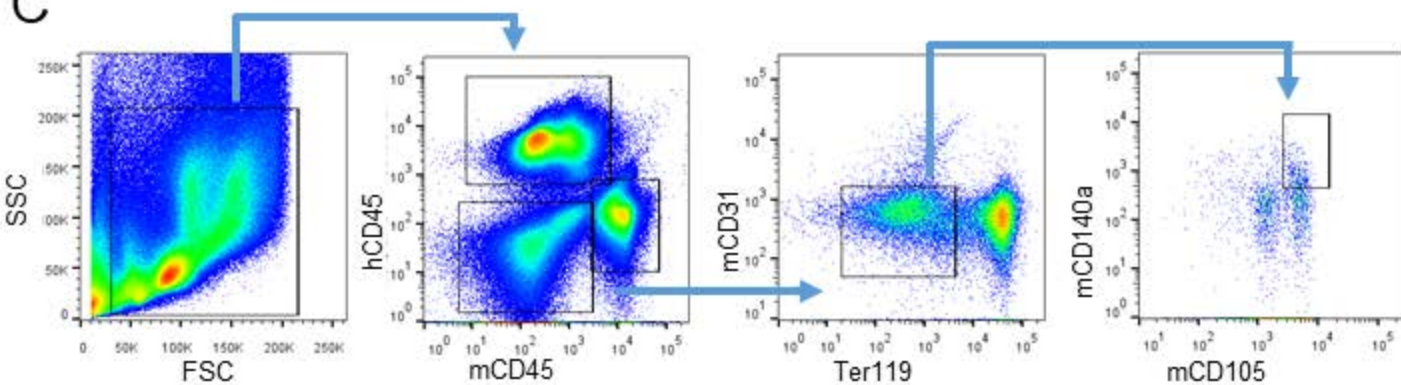
A



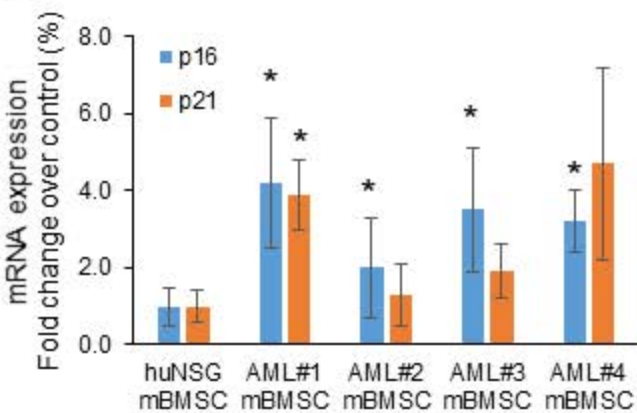
B



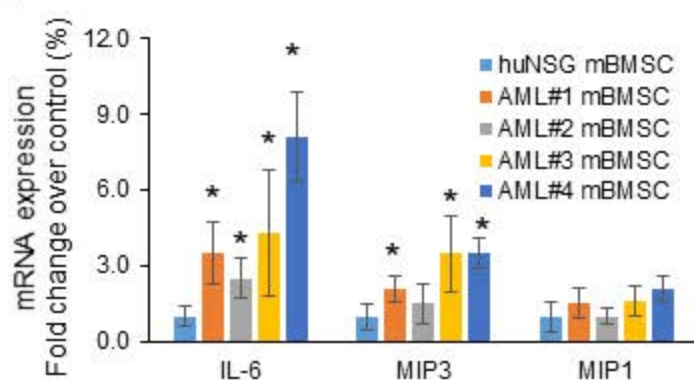
C



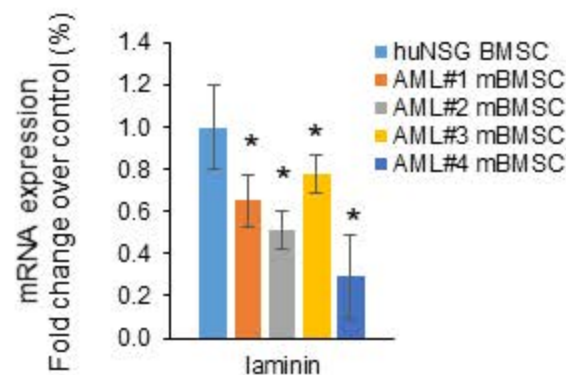
D



E



F



G

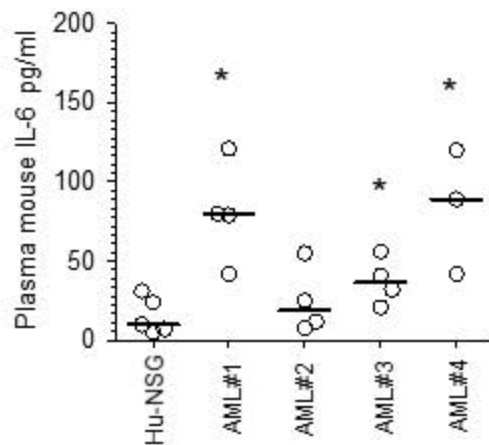


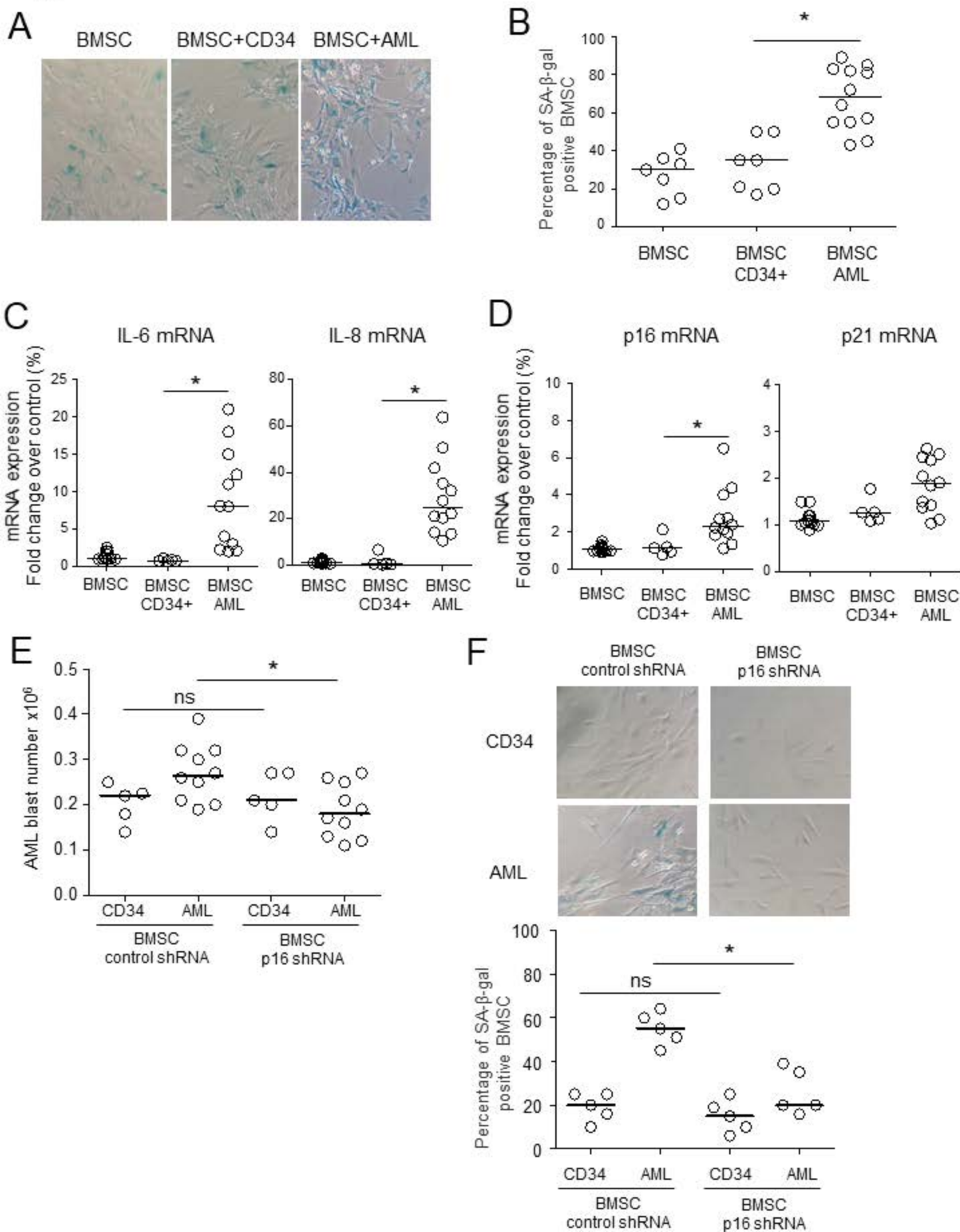
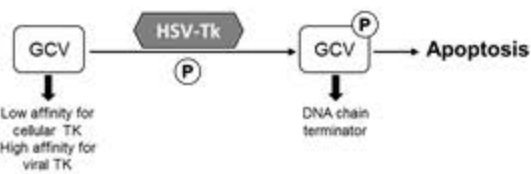
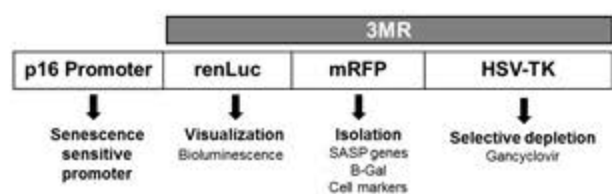
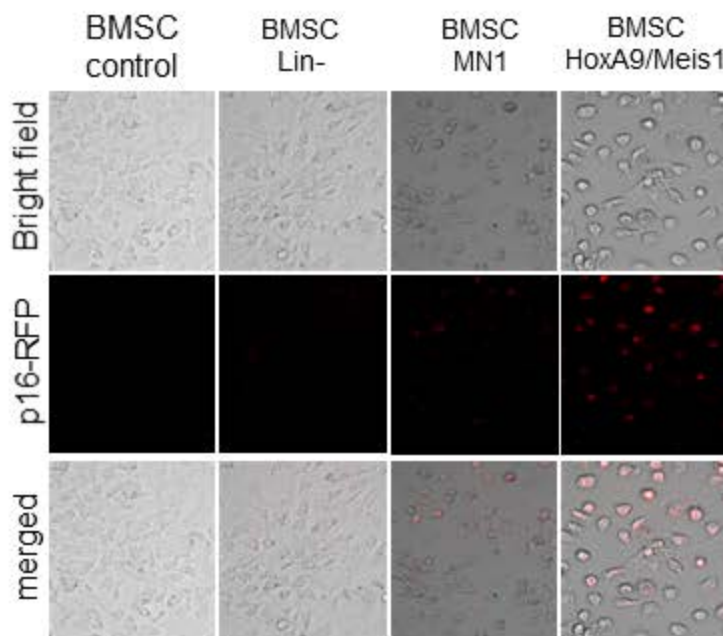
Figure 2.

Figure 3.

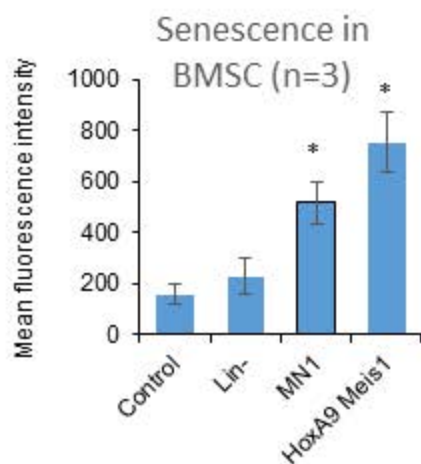
A



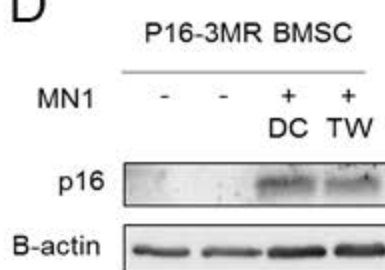
B



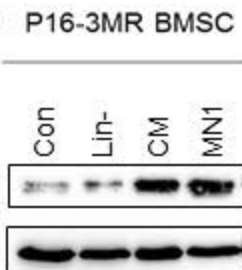
C



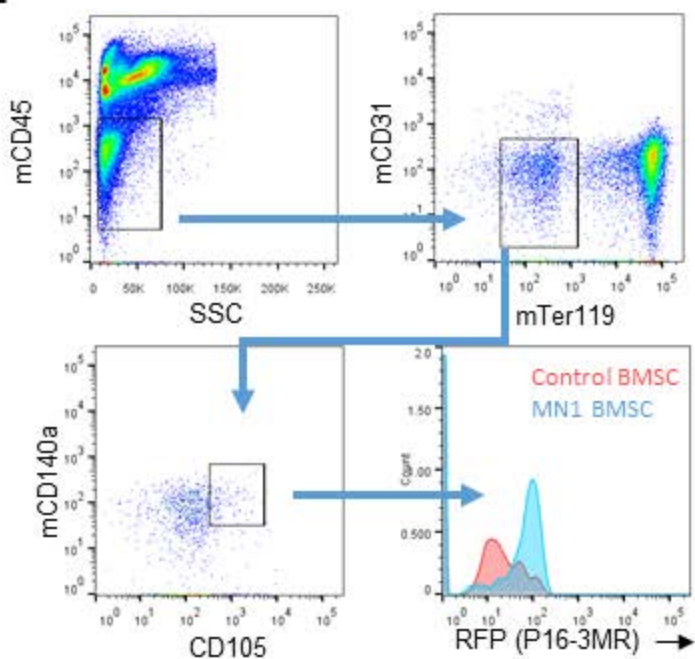
D



E



F



F

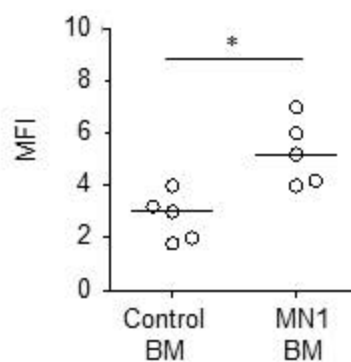
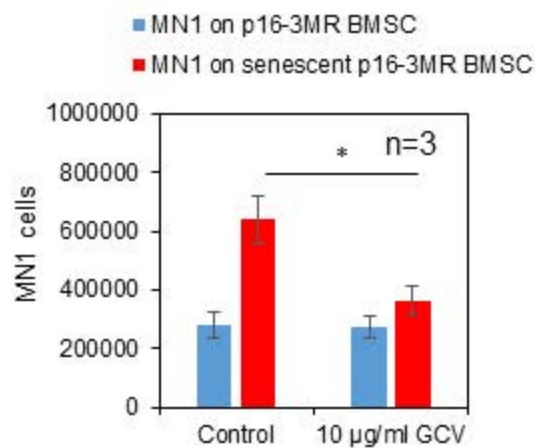
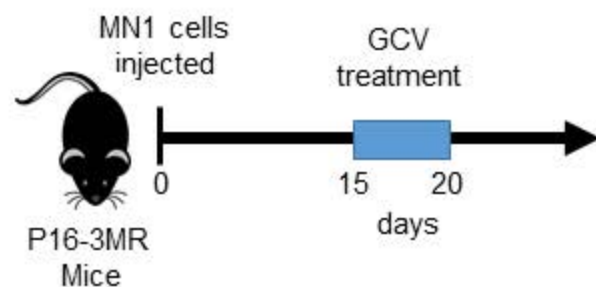


Figure 4

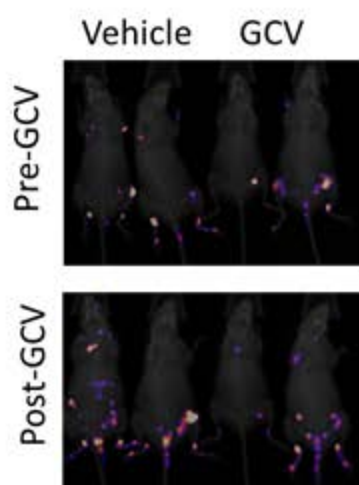
A



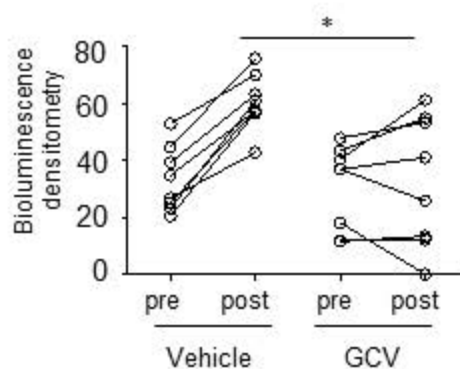
B



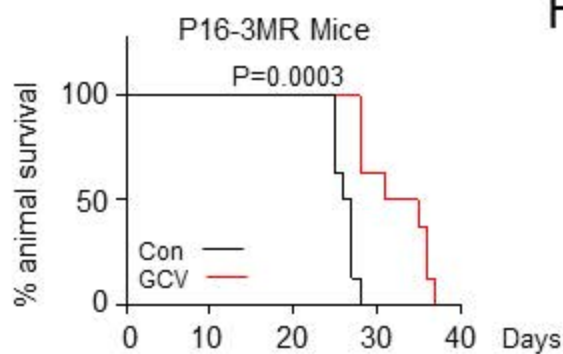
C



D



E



F

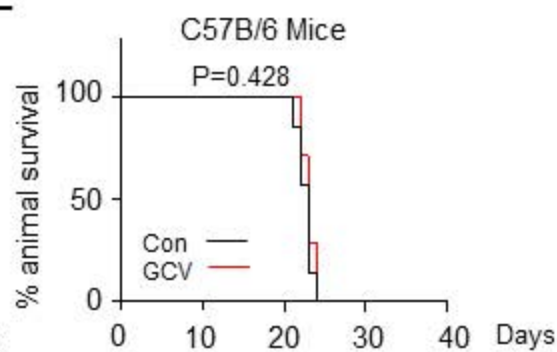


Figure 5

